Journal of Power Sources 198 (2012) 30–35

Contents lists available at SciVerse ScienceDirect

Journal of Power Sources

journal homepage: www.elsevier.com/locate/jpowsour

Platinum nanoparticles anchored on chelating group-modified graphene for methanol oxidation

Marzena S. Wietecha[a], Jun Zhu[b], Guihua Gao[b], Ning Wang[b], Huan Feng[c], Matthew L. Gorring[c], Marc L. Kasner[a], Shifeng Hou[a,*]

[a] Department of Chemistry & Biochemistry, Montclair State University, Montclair, NJ 07043, USA
[b] Department of Chemistry, Jining Medical College, Jining, Shandong Province 272113, PR China
[c] Department of Earth and Environment Studies, Montclair State University, Montclair, NJ 07043, USA

ARTICLE INFO

Article history:
Received 19 July 2011
Received in revised form
21 September 2011
Accepted 22 September 2011
Available online 29 September 2011

Keywords:
Platinum nanoparticles
Graphene oxide
Fuel cell
Electrochemical catalyst
Methanol

ABSTRACT

Platinum nanoparticles (Pt-NPs) were deposited onto N-(trimethoxy-silylpropyl) ethylenediamine triacetic acid (EDTA-silane) modified reduced graphene oxide (EDTA-RGO). The EDTA-RGO/Pt-NPs were coated onto a glass carbon electrode and characterized using scanning electron microscopy, transmission electron microscopy, X-ray diffraction, Raman spectra, and electrochemical tests. The chelating groups create a micro-environment that is suitable for the catalytic behavior of Pt-NPs. Compared with traditional carbon-based Pt catalysts, EDTA-RGO/Pt-NPs exhibit great tolerance towards poisoning by CO. Graphene-supported Pt nanoparticles can be used for the fabrication of fuel cell electrodes and other catalytic devices.

1. Introduction

Theoretically, direct methanol fuel cells are excellent power sources due to their high energy density, low pollutant emission, and easy handling. However, commercials applications are limited by the high cost related to fine metal catalysts and the poisoning caused by intermediate carbonaceous species. Significant efforts have been devoted to developing a series of carbon-supported catalysts for fuel cell electrodes with high catalytic activity, low cost, and high resistance to carbon monoxide (CO) poisoning [1–6]. The utilization of graphene as a two-dimensional support material to anchor nanoparticles (NPs) opens an avenue for the designing of the next generation of graphene-supported catalysts [7–26]. For example, one such application is to load metal NPs as an enhanced catalytic system for the oxidation of methanol in fuel cells. Recently, we have found that graphene oxide supported Pt and Pt–Ru nanoparticles possess high electrocatalytic activity for both methanol and ethanol oxidation [18]. Other researchers found that the presence of surface functional groups can improve wettability and accessibility of methanol to the electroactive surface [10]. These functional groups can act as nucleation centers or anchoring sites to limit particle growth, to improve the dispersion of metallic crystallites, and to enhance the stability of the supported catalysts [3,27–29].

Herein, we report the graphene functionalized with chelating groups and its application in loading Pt nanoparticles (Pt-NPs) for fuel cell applications. N-(trimethoxy-silylpropyl) ethylenediamine triacetic acid (EDTA-silane) can react with graphene oxide (GO) to form chelating groups modified graphene oxide (EDTA-GO) and then to form reduced chelating groups modified graphene oxide (EDTA-RGO). EDTA-GO and EDTA-RGO can be used as support materials for in situ synthesis of Pt nanoparticles. Our study shows that EDTA groups can anchor Pt-NPs on the graphene surface (defined as EDTA-RGO/Pt-NPs). The EDTA-RGO/Pt-NPs exhibit higher catalytic activity, longer stability, and excellent tolerance capability to CO poisoning. The results strongly indicate that graphene surface modified with the desired groups can dramatically enhance the surface properties of graphene which play a vital role in antipoisoning activity of Pt-NPs electrocatalysts.

2. Experimental

2.1. Equipment

The SEM images were taken on a Hitachi S3400 (Hitachi, Japan) with an energy dispersion X-ray (EDX) analyzer. The TEM images

* Corresponding author. Tel.: +1 973 655 7118.
E-mail address: hous@mail.montclair.edu (S. Hou).

0378-7753/$ – see front matter © 2011 Elsevier B.V. All rights reserved.
doi:10.1016/j.jpowsour.2011.09.073

were taken on a Hitachi H7000 (Hitachi, Japan). X-ray diffraction was taken on a Phillips X-Pert PRO powder diffractometer. The electrochemical tests were performed on CHI-660 electrochemical workstation (CHI Instruments Co., Texas) with a three-electrode system with a GC electrode as the working electrode (Φ = 3 mm), the saturated calomel electrode (SCE) as a reference electrode and a Pt wire as a counter electrode.

2.2. Materials

Graphite, hexachloroplatinic acid ($H_2PtCl_6{\cdot}xH_2O$), ethylene glycol (EG), $K_2S_2O_8$, P_2O_5, H_2SO_4, $KMnO_4$, Nafion, and 30% H_2O_2 were obtained from Aldrich and used without further purification. N-(Trimethoxysilylpropyl) ethylenediamine triacetic acid sodium salt (EDTA-Silane, 45% in water) was purchased from Gelest Inc. All of other reagents and solvents were directly used without further purification.

2.3. Procedures

Graphene oxide was synthesized using a modified Hummers method, while the silanization process of GO was accomplished by mixing GO with EDTA-silane in a methanol solution [30,31]. In a typical procedure, graphite powders were oxidized by sulphuric acid, $K_2S_2O_8$ and P_2O_5, the resulting material then was oxidized by concentrated H_2SO_4, $KMnO_4$, and 30% H_2O_2. After it was filtered and washed with 0.1 M HCl and by DI water, the graphene oxide (GO) dried in air was obtained.

The EDTA silane modified graphene oxide (EDTA-GO) was prepared by reacting 1.0 ml N-(trimethoxysilylpropyl) ethylenediamine triacetic acid (EDTA-silane) with 1.0 g GO in 200 ml methanol through a silylation process [31]. The product (EDTA-GO) was isolated by filtration and washed with methanol and water sequentially. The molar ratio of Si to C in the EDTA-GO products was determined to be 1:(12.7 ± 2.2).

The synthetic route to obtain the EDTA-GO supported Pt-NPs (EDTA-RGO/Pt-NPs) is illustrated in Fig. 1. In our experiment, the synthesis of Pt-NPs was completed by mixing EDTA-GO powder with hexachloroplatinic acid ($H_2PtCl_6{\cdot}xH_2O$) in an ethylene glycol (EG) solution and then the solution was refluxed under argon protection at 140 °C for 4 h. We observed that the mass ratio of EDTA-GO to H_2PtCl_6 varied from 1:0.1 to 1:0.5. The reduction of H_2PtCl_6 to Pt-NPs and reduction of the graphene oxide to reduced graphene oxide (RGO) were completed during the refluxing process [10]. EDTA-RGO/Pt-NPs was isolated by filtration and washed with methanol and water sequentially. Finally, the product was dried in a vacuum oven at 120 °C for 12 h, and this treatment procedure can enhance the catalytic activity of EDTA-RGO/Pt-NPs for the oxidation of methanol [19].

As a control experiment, RGO/Pt-NPs was synthesized by mixing GO powder with hexachloroplatinic acid ($H_2PtCl_6{\cdot}xH_2O$) in an ethylene glycol (EG) solution, and then the solution was fluxed under constant argon flow at 140 °C for 4 h. The mass ratio of RGO to H_2PtCl_6 varies from 1:0.1 to 1:0.5. And all of other procedures are performed at the same condition mentioned above. The chemical reduction of GO to RGO was obtained by mixing GO with ethylene glycol–water solution without metallic salts and then the solution was fluxed under constant argon flow at 140 °C for 4 h. All of the other treatment procedures are the same as mentioned above.

2.4. Characterization

GO, RGO, EDTA-RGO, RGO/Pt-NPs and EDTA-RGO/Pt-NPs were characterized using X-ray diffraction (XRD), scanning electron microscopy (SEM) and Raman spectroscopy.

To fabricate a working electrode, 10 mg of EDTA-RGO/Pt-NPs were initially dispersed in 5.0 ml 0.5% Nafion ethanol solution and then stirred for 24 h to entirely disperse EDTA-RGO/Pt-NPs into Nafion ethanol solution. Nafion is used as an adhesive to affix the catalysts to the electrode surface. Then, 10 μl of this suspension was placed onto the surface of a glassy carbon (GC) electrode and dried. Finally, another 10 μl 0.2% Nafion ethanol solution was applied and dried. This as-prepared electrode was defined as EDTA-RGO/Pt-NPs/GC electrode. As a control experiment, RGO/Pt-NPs coated GC electrode was prepared with the same procedure and it was defined as RGO/Pt-NPs/GC electrode. Electrocatalytic oxidation of methanol was measured in a 0.50 M CH_3OH + 0.50 M H_2SO_4 solution by cyclic voltammetry (CV) between −0.2 V and 1.20 V at room temperature.

3. Results and discussion

3.1. Characterization of EDTA-RGO/Pt-NPs

3.1.1. SEM and TEM

Fig. 2a is a typical SEM image of EDTA-RGO/Pt-NPs powders and Fig. 2b depicts the elemental compositions of the EDTA-RGO/Pt-NPs through energy dispersive X-ray spectroscopy (EDXS). The existence of Si and Pt on EDTA-RGO/Pt-NPs is indicated by the presence of Si signal at 1.74 keV and Pt signal at 2.05 and 9.44 keV, respectively. Fig. 3a is a typical TEM image of EDTA-RGO/Pt-NPs, with the graphene sheets clearly shown. Fig. 3b is a high resolution TEM image of EDTA-RGO/Pt-NPs. Pt-NPs in Fig. 3b are in the size range of 2.2–4.6 nm.

3.1.2. XRD

The X-ray diffraction (XRD) patterns of EDTA-GO, EDTA-RGO/Pt-NPs and a commercial Pt reference catalyst (Pt-loaded graphite, 5 wt% Pt) are shown in Fig. 4a. Generally, the graphite sample has two diffraction peaks at 25.90° and 53.6°, which are assigned to the graphite crystalline planes C (0 0 2) and C (0 0 4), respectively. Compared EDTA-GO sample with graphite, these two peaks disappear, while a new broad peak (GO peak, plane C (0 0 2)/GO) at 2θ = 10.29° with ~0.78 nm d-spacing is shown. With the formation of EDTA-RGO/Pt-NPs, the GO peak almost disappeared while a new broad graphite peak with low intensity appeared at 24.52°. This peak can be assigned to C (0 0 2) graphite peak. These observations suggest that, in a reducing process, the conjugated graphene network (sp^2 carbon) has been re-established. This is consistent with the peak appearance of reduced graphene oxide [8]. Fig. 4a shows the characteristic diffraction peaks of Pt (1 1 1) for EDTA-RGO/Pt-NPs and Pt-loaded graphite at 39.6°. Both samples also have the characteristic diffraction peaks of Pt (2 0 0) at 46.2°, and Pt (2 2 0) at 67.5°.

The diffraction peak for Pt (2 2 0) is used to estimate the Pt-NPs size with the Scherrer equation, because there is no interference from other diffraction peaks, and the average size of Pt-NPs in our system is about 2.8 nm [8,29]. However, comparing the XRD of EDTA-RGO/Pt-NPs with Pt-loaded graphite, there is no more interference peak at Pt (2 0 0) band at 46.3° of EDTA-RGO/Pt-NPs. These data demonstrate that the crystallinity of Pt-NPs formed on EDTA-RGO surface is uniform. It is also evident that the sharper Pt (1 1 1) peak (Fig. 3a) indicates the higher loading capacity of Pt-NPs with an EDTA-surface.

3.1.3. Raman spectra

Fig. 4b shows the Raman spectra of EDTA-GO, EDTA-RGO and EDTA-RGO/Pt-NPs. A broad G-band at 1592–1598 cm^{-1} is found for EDTA-GO (1596 cm^{-1}), EDTA-RGO (1593 cm^{-1}) and EDTA-RGO (1592 cm^{-1}), respectively. This peak is attributed from the sp^2-hybridizaed carbon atoms in graphene sheet. The peak at about

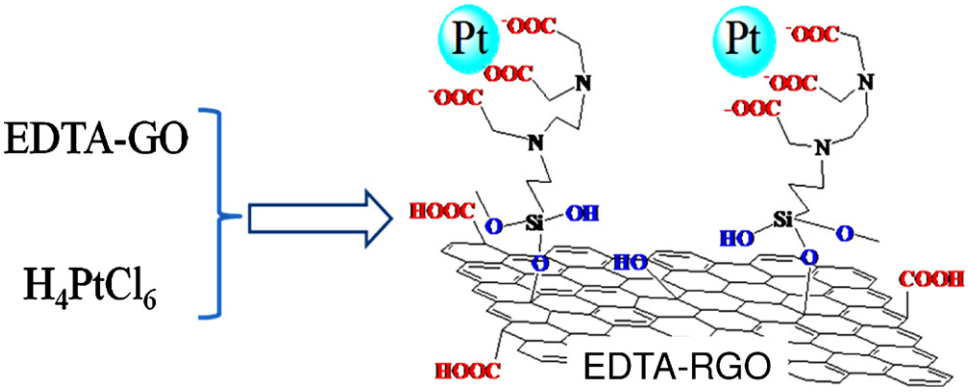

Fig. 1. The scheme to load Pt nanoparticles on EDTA-GO surface.

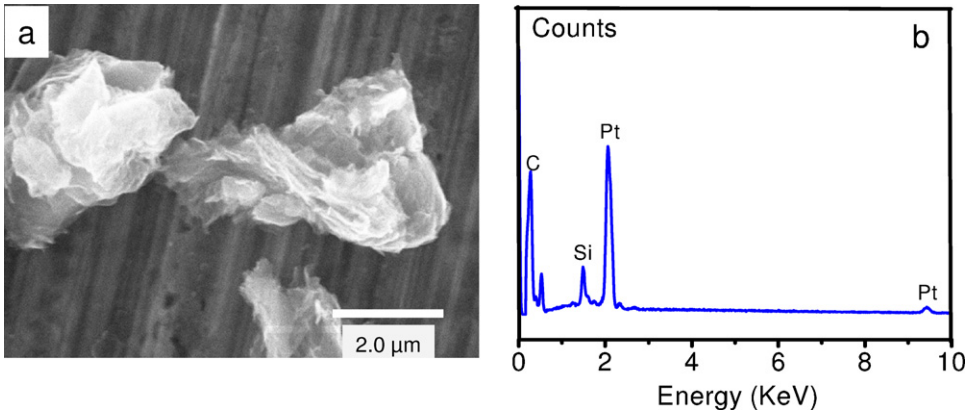

Fig. 2. The SEM image (a) and EDXS (b) of EDTA-RGO/Pt-NPs.

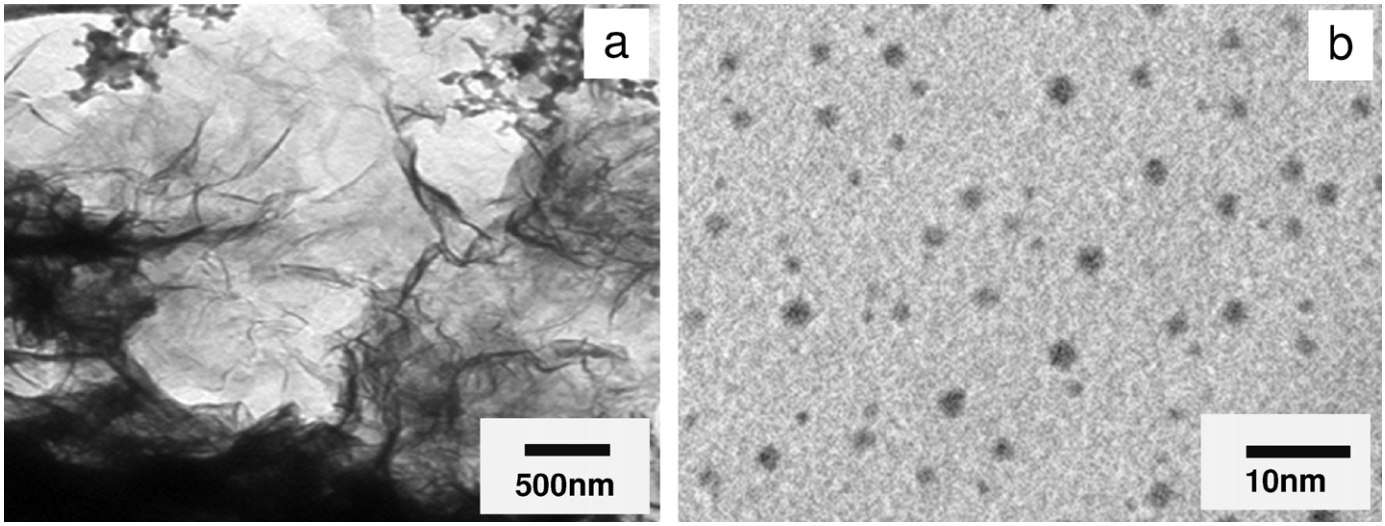

Fig. 3. The TEM image of EDTA-RGO/Pt-NPs.

1352 cm^{-1} is the oxidation of disruption of the sp^2-hybridized carbon atoms. After the reduction of the EDTA-GO to EDTA-RGO, the G band shifts from 1596 cm^{-1} to 1593 cm^{-1}, indicating that the production of RGO. For EDTA-RGO/Pt-NPs, the G band shifts to even lower 1592 cm^{-1}. It is obvious that there is a decrease in the average domain size of the sp^2-hybridized carbon atoms with the increase of the D/G intensity ratio in EDTA-RGO/Pt-NPs.

3.2. Electrochemical catalysis behavior towards the oxidation of methanol

3.2.1. Cyclic voltammetry

Electrochemical catalytic behavior of EDTA-RGO/Pt-NPs/GC electrode towards the oxidation of methanol was examined by CV. To compare the catalytic activities of Pt-NPs on RGO and

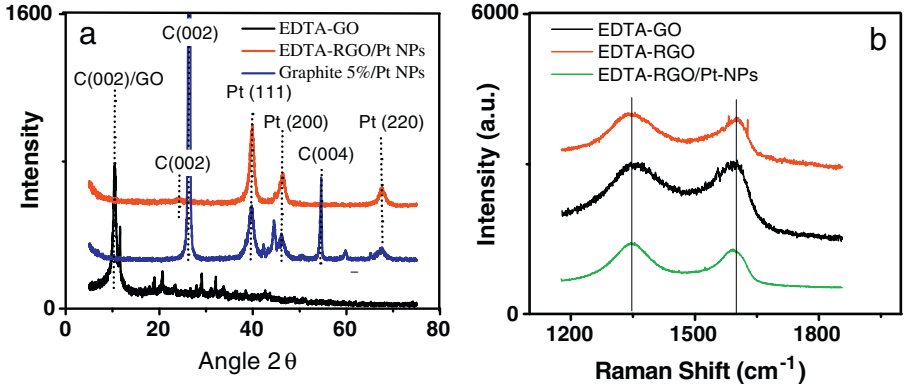

Fig. 4. The XRD of EDTA-GO, EDTA-RGO/Pt-NPs and Graphite-Pt-NPs (a), and the Raman spectra of EDTA-GO, EDTA-RGO and EDTA-RGO/Pt-NPs (b).

EDTA-GO surfaces, CV process was performed at room temperature (25 ± 1) °C, and the scan rate of two electrodes was fixed at 60 mV s^{-1}, and the solution was a 0.5 M methanol + 0.5 M H_2SO_4 solution. The potential scan started at −0.2 V and ended at 1.2 V (forward potential scan) and then back from 1.2 V to −0.2 V (reverse potential scan). The presented cyclic voltammograms are shown in Fig. 5. When the scan is from −0.2 V to 1.2 V, the oxidation peak of methanol appears at 0.67 V and the peak current density is defined as the forward anodic peak current density (I_f). In the reverse potential scan, the scan is back from 1.2 V to −0.2 V, a peak appears at ~0.5 V, the peak current density is designated as the reverse (or backward) anodic peak current density (I_b). The reverse anodic peak is attributed to the oxidation of CO_{ads}-like species, and it is believed that these species are generated from the incomplete oxidation of methanol during the forward potential scan.

The observed I_f of methanol oxidation on an EDTA-RGO/Pt-NPs/GC electrode is approximately 6.3 mA cm^{-2}. The observed I_f of methanol oxidation on a RGO/Pt-NPs/GC electrode is approximately 4.2 mA cm^{-2}, which is only ~65% of that on the EDTA-RGO/Pt-NPs/GC electrode, indicating an enhanced methanol oxidation activity for the EDTA-RGO/Pt-NPs/GC electrode. From Fig. 5, the observed I_b of CO_{ads}-like species oxidation on the EDTA-RGO/Pt-NPs/GC electrode is approximately 1.9 mA cm^{-2}. The observed I_b of CO_{ads}-like species oxidation on the RGO/Pt-NPs/GC electrode is approximately 3.9 mA cm^{-2}, which is higher than that on the EDTA-RGO/Pt-NPs/GC electrode. These results predict that fewer CO_{ads}-like species are generated on the EDTA-RGO/Pt-NPs electrode, because of that the higher I_b indicating an incomplete methanol oxidation process.

In addition, Fig. 6a depicts that the cyclic voltammogram of EDTA-RGO/Pt-NPs/GC electrode to methanol oxidation at different scan rates while Fig. 6b demonstrates that the I_f is positively proportional to the square root of the scan rate, suggesting that the oxidation of methanol at electrode is a diffusion or a semi-infinite linear diffusion controlled process.

3.2.2. Tolerance to CO poisoning

The magnitude of the peak current density is directly proportional to the amount of methanol oxidized at the electrode. The ratio of I_f to I_b can be used to explain the catalyst tolerance to CO and other carbonaceous species. Fig. 7 shows that the I_f/I_b ratio values decrease as the scan rate increase, indicating that the CO accumulation increases with an increasing scan rate. Furthermore, investigation demonstrates that, EDTA-RGO/Pt-NPs displaying much higher I_f/I_b ratios compared to RGO/Pt-NPs at five scan rates (20, 40, 60, 80 and 100 mV s^{-1}), indicating superior antipoisoning behavior. This result suggest that EDTA-GO supported Pt-NPs may lead to a more complete methanol oxidation to CO. Compared with carbon black supported Pt-NPs, EDTA-RGO/Pt-NPs have a ratio of 2.0 to 2.6 (at scan rate 60 mV s^{-1}), which is much higher than that of carbon black (1.39), graphite (1.03) [29]. The finding suggests that not only graphene bus also EDTA chelating groups play a critical role of Pt-NPs in the catalytic behavior in the accelerating the methanol oxidation in the anti-poisoning of CO.

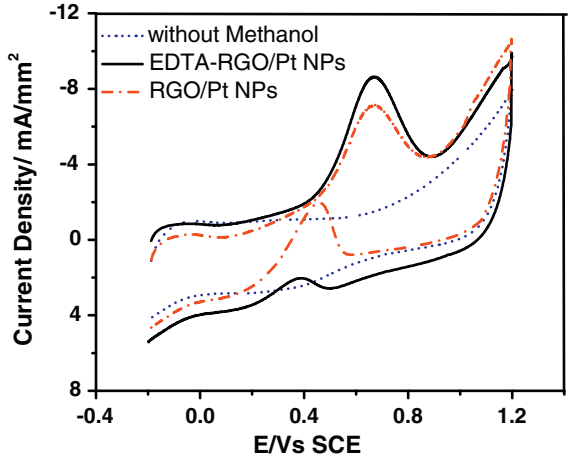

Fig. 5. The cyclic voltammogram of EDTA-RGO/Pt-NPs/GC electrode in 0.5 M bulk H_2SO_4 solution and in methanol solution (0.5 M methanol + 0.5 M H_2SO_4) and GO/Pt-NPs/GC in the same methanol solution. Scan rate 60 mV s^{-1}.

3.3. Stabilities of EDTA-RGO/Pt-NPs

A major concern in current fuel-cell technology stems from the stability of catalysts that is a critical parameter for evaluation of anode materials. To investigate the stability of EDTA-RGO/Pt-NPs/GC electrode towards the oxidation of methanol, cyclic voltammetry was used to test the stability of Pt-NPs catalysis behavior towards the oxidation of methanol. As shown in Fig. 8, I_f after 400 CV cycles is ~80% of the initial I_f values, the EDTA-RGO/Pt-NPs/GC electrode exhibits a stable forward current. Although the initial decay occurs because of the formation of intermediate species such as CO_{ads}, CH_3OH_{ads}, and CHO_{ads} during the oxidation, the decay rate is much slower than the most graphite supported Pt-NPs [32].

Our experiment has demonstrated that the presence of EDTA groups on RGO surface plays a critical role in the catalytic activities of Pt-NPs. The presence of EDTA groups can significantly enhance the electrocatalytic activity of Pt-NPs for methanol oxidation to CO_2, and the EDTA groups can more effectively enhance CO-poisoning tolerance. To analyze the potential mechanisms, we

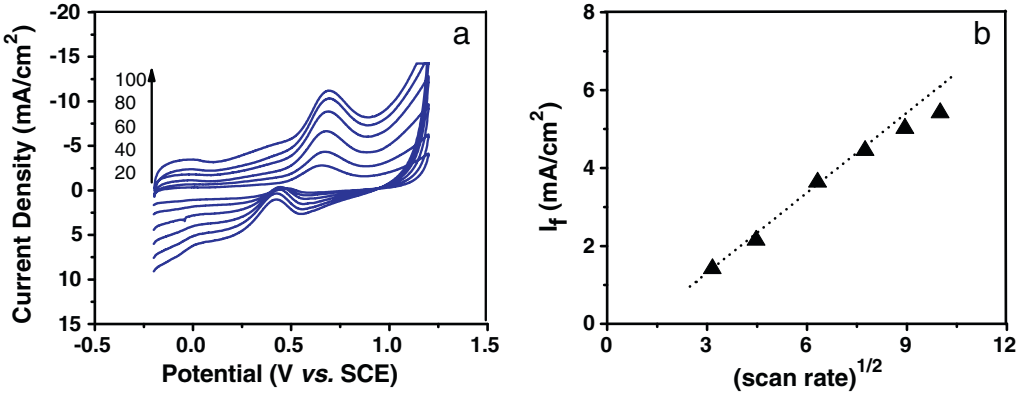

Fig. 6. The cyclic voltammogram of EDTA-RGO/Pt-NPs/GC electrode to methanol oxidation at different scan rates (from bottom: 20, 40, 60, 80, 100 mV s^{-1}) (a), and the relationship of I_f vs. the square root of scan rate (b).

need to investigate the effect of the substrate surface groups on the catalytic properties of the Pt-NPs. It has been demonstrated that the oxygen groups on the graphene substrate surface can promote the oxidation of CO adsorbed [8]. In addition, the thermodynamic analysis has proved that nitrogen (or boron) doped graphene improves CO tolerance of Pt nanoparticles and the strong binding of Pt nanoparticles on defective graphene leads to enhancing the stability [33–35]. Thus, the anti-poisoning capability of

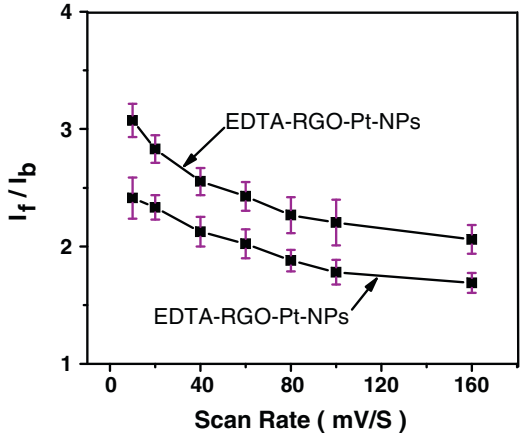

Fig. 7. The relationship of I_f/I_b ratio vs. scan rate of RGO/Pt-NPs/GC and EDTA-RGO/Pt-NPs electrodes.

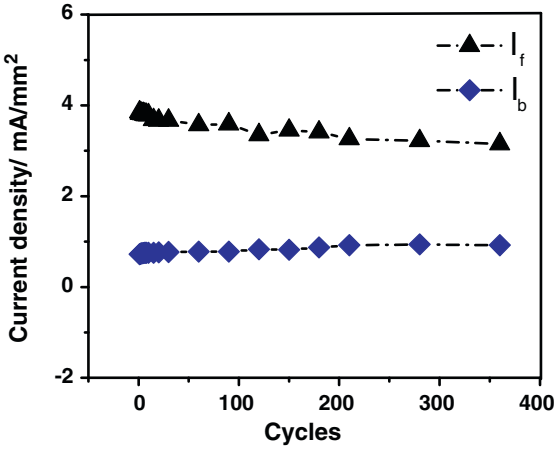

Fig. 8. The relationship of I_f and I_b vs. the scan cycles of EDTA-RGO/Pt-NPs/GC electrode, scan rate 50 mV s^{-1}, solution: 0.5 M methanol + 0.5 M H_2SO_4.

Pt-based nanoparticals towards CO_{ads} dependents on the surface groups, the group types and the group surface densities of substrate. On EDTA-RGO surface, the EDTA group contributes not only nitrogen atoms, but also –OH and –COOH groups. These groups provide a strong binding to anchor Pt-NPs, and create a hydrophilic microenvironment, which may also enhance the anti-poisoning properties of EDTA-RGO/Pt-NPs. The possible mechanisms of the effects of the EDTA groups on the activity of Pt-NPs are as follows: First, Pt metal ions can form a complex with the carboxyl anions and amine groups. In the fabrications process, the presence of EDTA on GO surface can control the nanoparticle size, narrow the particle size distribution and prevent the Pt-NPs from aggregation (see Fig. 3b) [36]. Second, after the fabrication of Pt-NPs of EDTA-RGO surface, EDTA plays several roles in enhancing the performance of Pt-NPs catalysis properties, (1) EDTA had three carboxyl anions and two nitrogen-containing groups. Hence, there is a complex interaction between the EDTA groups and Pt-NPs. This complex interaction can exert steric hindrance and coulombic effects on the metal particles, thereby stabilizing Pt-NPs. The strong interaction between Pt-NPs and EDTA can induce modulation in the electronic structure of Pt-NPs, control the structure and shape of the NPs, lower the Pt–CO binding energy and thus reduce the CO adsorption on Pt [33,36,37]; (2) the presence of EDTA groups enhances the hydrophilic properties of RGO and thus promotes water activation. As a result, the adsorbed OH^- species at the Pt-NPs promote the oxidation of CO [8,36]; (3) the EDTA groups can provide additional reaction sites, like most nitrogen substituted graphene, to bind Pt-NPs, to stabilize the Pt-NPs against coarsening, and then to enhance the stability and efficient of Pt-NPs; (4) the EDTA groups can enhance charge transfer between the reactants and electrode [36].

In addition, our data also indicate that the I_f current decay rates are improportional to mass ratio of EDTA-RGO to loaded Pt-NPs. A possible explanation is that a result of that the Pt-NPs on EDTA-RGO surface may have been divided into two groups with the increase of the Pt-NPs density. One group contains all Pt-NPs that can interact with EDTA groups directly (binding-groups), while the other group has Pt-NPs that have no interaction with EDTA-groups (non-binding groups). With more and more Pt-NPs deposited onto EDTA-RGO surface, the EDTA-sites are taken by Pt-NPs. The later formed Pt-NPs will deposit onto graphene surface directly. These Pt-NPs cannot be protected by EDTA groups and exhibit less tolerance towards the CO poisoning. The more Pt-NPs deposited on EDTA-RGO surface, the lower ratio of binding-Pt-NPs and, hence, the lower tolerance towards CO poisoning. To obtain the best performance of EDTA-RGO support Pt-NPs catalysts for fuel cell applications, more works are needed to optimize the relationship among the stability of EDTA-RGO/Pt-NPs, the surface density of EDTA groups and loaded Pt-NPs on EDTA-RGO surface.

4. Conclusion

Our research demonstrates that Pt-NPs can be synthesized on the functionalized graphene surface with chelating groups and proves that the chelating groups can enhance the catalytic activities of Pt-NPs towards the oxidation of methanol. In addition, these Pt-NPs on EDTA-RGO surface exhibit high stability. The ratio of I_f/I_b of the EDTA-RGO/Pt-NPs/GC electrode towards methanol oxidation is much higher than that of the commercial Pt/C catalysts, carbon nanotubes, and graphene-supported Pt catalysts. The technique developed in this study can be extended to synthesize various functionalized graphenes with other functional groups, thus providing a general route for preparing multifunctional graphene as a support for various catalysis applications. Further investigations should be focused on carefully controlling the particles sizes, facets, and size distributions, which is expected to result in the next generation of grapheme-supported catalytic systems that not only for fuel cells, but also for other catalytic systems.

Acknowledgment

This work was supported by the Sokol Institute Fellows Program.

References

[1] X.Z. Cui, L.M. Guo, F.M. Cui, Q.J. He, J.L. Shi, J. Phys. Chem. C 113 (2009) 4134–4138.
[2] S. Kim, H.J. Sohn, S.J. Park, Curr. Appl. Phys. 10 (2010) 1142–1147.
[3] R.V. Hull, L. Li, Y.C. Xing, C.C. Chusuei, Chem. Mater. 18 (2006) 1780–1788.
[4] T. Takeguchi, Y. Anzai, R. Kikuchi, K. Eguchi, W. Ueda, J. Electrochem. Soc. 154 (2007) B1132–B1137.
[5] G.Q. Lu, W. Chrzanowski, A. Wieckowski, J. Phys. Chem. B 104 (2000) 5566–5572.
[6] Z. Jusys, R.J. Behm, J. Phys. Chem. B 105 (2001) 10874–10883.
[7] S.J. Guo, S.J. Dong, E.K. Wang, ACS Nano 4 (2010) 547–555.
[8] S. Sharma, A. Ganguly, P. Papakonstantinou, X.P. Miao, M.X. Li, J.L. Hutchison, M. Delichatsios, S. Ukleja, J. Phys. Chem. C 114 (2010) 19459–19466.
[9] B. Seger, P.V. Kamat, J. Phys. Chem. C 113 (2009) 7990–7995.
[10] Y.J. Li, W. Gao, L.J. Ci, C.M. Wang, P.M. Ajayan, Carbon 48 (2010) 1124–1130.
[11] S. Liu, J.Q. Wang, J. Zeng, J.F. Ou, Z.P. Li, X.H. Liu, S.R. Yang, J. Power Sources 195 (2010) 4628–4633.
[12] N.G. Shang, P. Papakonstantinou, P. Wang, S. Ravi, P. Silva, J. Phys. Chem. C 114 (2010) 15837–15841.
[13] Y.Y. Shao, S. Zhang, C.M. Wang, Z.M. Nie, J. Liu, Y. Wang, Y.H. Lin, J. Power Sources 195 (2010) 4600–4605.
[14] S. Zhang, Y.Y. Shao, H.G. Liao, J. Liu, I.A. Aksay, G.P. Yin, Y.H. Lin, Chem. Mater. 23 (2011) 1079–1081.
[15] Y.J. Hu, J.A. Jin, P. Wu, H. Zhang, C.X. Cai, Electrochim. Acta 56 (2010) 491–500.
[16] C. Xu, X. Wang, J.W. Zhu, J. Phys. Chem. C 112 (2008) 19841–19845.
[17] N. Li, Z.Y. Wang, K.K. Zhao, Z.J. Shi, S.K. Xu, Z.N. Gu, J. Nanosci. Nanotechnol. 10 (2010) 6748–6751.
[18] L.F. Dong, R.R.S. Gari, Z. Li, M.M. Craig, S.F. Hou, Carbon 48 (2010) 781–787.
[19] Y.C. Xin, J.G. Liu, Y. Zhou, W.M. Liu, J.A. Gao, Y. Xie, Y. Yin, Z.G. Zou, J. Power Sources 196 (2011) 1012–1018.
[20] S.Y. Wang, X. Wang, S.P. Jiang, Phys. Chem. Chem. Phys. 13 (2011) 7187–7195.
[21] E. Yoo, T. Okada, T. Akita, M. Kohyama, I. Honma, J. Nakamura, J. Power Sources 196 (2011) 110–115.
[22] J. Oh, E. Yo, C. Ono, T. Kizuka, T. Okada, J. Nakamura, J. Power Sources 185 (2008) 886–891.
[23] G.X. Zhang, S.H. Sun, D.Q. Yang, J.P. Dodelet, E. Sacher, Carbon 46 (2008) 196–205.
[24] C.V. Rao, A.L.M. Reddy, Y. Ishikawa, P.M. Ajayan, Carbon 49 (2011) 931–936.
[25] F.H. Li, J. Chai, H.F. Yang, D.X. Han, L. Niu, Talanta 81 (2010) 1063–1068.
[26] G. Wu, D.Y. Li, C.S. Dai, D.L. Wang, N. Li, Langmuir 24 (2008) 3566–3575.
[27] R.I. Jafri, N. Rajalakshmi, S. Ramaprabhu, J. Mater. Chem. 20 (2010) 7114–7117.
[28] S.Y. Wang, F. Yang, S.P. Jiang, S.L. Chen, X. Wang, Electrochem. Commun. 12 (2010) 1646–1649.
[29] Y.L. Hsin, K.C. Hwang, C.T. Yeh, J. Am. Chem. Soc. 129 (2007) 9999–10010.
[30] S.F. Hou, M.L. Kasner, S.J. Su, K. Patel, R. Cuellari, J. Phys. Chem. C 114 (2010) 14915–14921.
[31] S.F. Hou, S.J. Su, M.L. Kasner, P. Shah, K. Patel, C.J. Madarang, Chem. Phys. Lett. 501 (2010) 68–74.
[32] A. Perez, M.J. Vilkas, C.R. Cabrera, Y. Ishikawa, J. Phys. Chem. B 109 (2005) 23571–23578.
[33] G. Kim, S.H. Jhi, ACS Nano 5 (2011) 805–810.
[34] R.T. Lv, T.X. Cui, M.S. Jun, Q. Zhang, A.Y. Cao, D.S. Su, Z.J. Zhang, S.H. Yoon, J. Miyawaki, I. Mochida, F.Y. Kang, Adv. Funct. Mater. 21 (2011) 999–1006.
[35] C.K. Acharya, C.H. Turner, Surf. Sci. 602 (2008) 3595–3602.
[36] J.-M. Liu, H. Meng, J.-L. Li, S.-J. Liao, J.-H. Bu, Fuel Cell 7 (2007) 402–407.
[37] C. Nethravathi, E.A. Anumol, M. Rajamathi, N. Ravishankar, Nanoscale 3 (2011) 569–571.